Biosensors and Bioelectronics 145 (2019) 111708

Contents lists available at ScienceDirect

Biosensors and Bioelectronics

journal homepage: www.elsevier.com/locate/bios

Extracellular electrophysiological based sensor to monitor cancer cells cooperative migration and cell-cell connections

Sanaz Asgarifar[a,b,1], Ana L.G. Mestre[a,b,1], Rute C. Félix[c], Pedro M.C. Inácio[a,b], Maria L.S. Cristiano[a,c], Maria C.R. Medeiros[d], Inês M. Araújo[e,f,g], Deborah M. Power[a,c], Henrique L. Gomes[a,b,*]

[a] Universidade do Algarve, Faculdade de Ciências e Tecnologia, 8005-139, Faro, Portugal
[b] Instituto de Telecomunicações, Avenida Rovisco, Pais 1, 1049-001, Lisboa, Portugal
[c] Centro de Ciências do Mar, Universidade do Algarve, 8005-139, Faro, Portugal
[d] Instituto de Telecomunicações, Departamento de Engenharia Electrotécnica e Computadores, Universidade de Coimbra, 3030-290, Coimbra, Portugal
[e] Centro de Investigação em Biomedicina, Universidade do Algarve, 8005-139, Faro, Portugal
[f] Departamento de Ciências Biomédicas e Medicina, Universidade do Algarve, 8005-139, Faro, Portugal
[g] Algarve Biomedical Center, Universidade do Algarve, 8005-139, Faro, Portugal

ARTICLE INFO

Keywords:
Cell-based biosensor
Extracellular
Electrophysiological
Cell-cell interactions
Migration
Signal synchronization

ABSTRACT

Herein, we describe an electrophysiological based sensor that reproducibly monitors and quantifies in real-time collective migration and the formation of cell-cell junctions by C6 glioma cells seeded on top of electrodes. The signal amplitude and frequency generated by the migrating cells changed over time and these parameters were used to accurately calculate the migration speed. Electrophysiological measurements could also distinguish individual from collective cell migration. The migration of densely packed cells generated strong signals, while dispersed cells showed weak bioelectrical activity. We propose this electrophysiological technique as a cell-based biosensor to gain insight into the mechanisms of cooperative migration of cancer cells. Possible applications include screening for anti-migratory compounds, which may lead to the development of novel strategies for antineoplastic chemotherapy.

1. Introduction

Cell-based biosensors have been utilized for cellular physiological analysis, pharmaceutical evaluation, environmental monitoring and medical diagnosis (Banerjee and Bhunia, 2010; DeBusschere and Kovacs, 2001; Johnstone et al., 2010; Pan et al., 2019; Pancrazio and Borkholder, 1999; Ye et al., 2019). Electrogenic cells or tissues are cultured on top of microelectrode arrays known as MEAS (Hierlemann et al., 2011). Extracellular potential changes can be monitored to assess the influence of drugs on cellular activities. Following the pioneering work of Gross (Gross et al., 1995) who used neuronal networks seeded on MEAS, some other electrogenic cells and tissues, such as cardiomyocytes, brain slices and retinal networks, are also gradually becoming acceptable as pharmacological models (Spira and Hai, 2013). Recently, we (Medeiros et al., 2016; Rocha et al., 2016) and others (Cabello et al., 2019) reported that populations of non-electrogenic or non-excitable cells such as cancer cells and astrocytes (Mestre et al., 2017b, 2017a) synchronize their activity and generate discrete bioelectrical signals. This type of sensing device differs from conventional MEAS because they are comparatively large area devices and therefore do not have the spatial resolution to measure individual action potentials. Furthermore, these sensing electrodes together with non-invasive electrophysiological measuring techniques can be used as cell-based biosensors to study cooperative activity in non-excitable cells.

A highly relevant biological problem in which cell-cell cooperation occurs is cell migration and in particular cell migration during cancer metastasis. Cancer cells are capable of synchronizing their signaling apparatus, thus cooperating to migrate and invade. Ion channels and ionic waves may have an important role when cells move as coherent groups. This type of migration is known as collective cell migration (Gov, 2014; Jiang et al., 2015; Theveneau and Mayor, 2012). The underlying cellular and molecular mechanisms of collective migration include cell-cell adhesion, force generation and orientation. The regulation of these interactions requires the coordination of a multiplicity

* Corresponding author. Universidade do Algarve, Faculdade de Ciências e Tecnologia, 8005-139, Faro, Portugal.
E-mail address: hgomes@ualg.pt (H.L. Gomes).
[1] Equally contributed.

https://doi.org/10.1016/j.bios.2019.111708
Received 18 August 2019; Accepted 15 September 2019
Available online 17 September 2019
0956-5663/

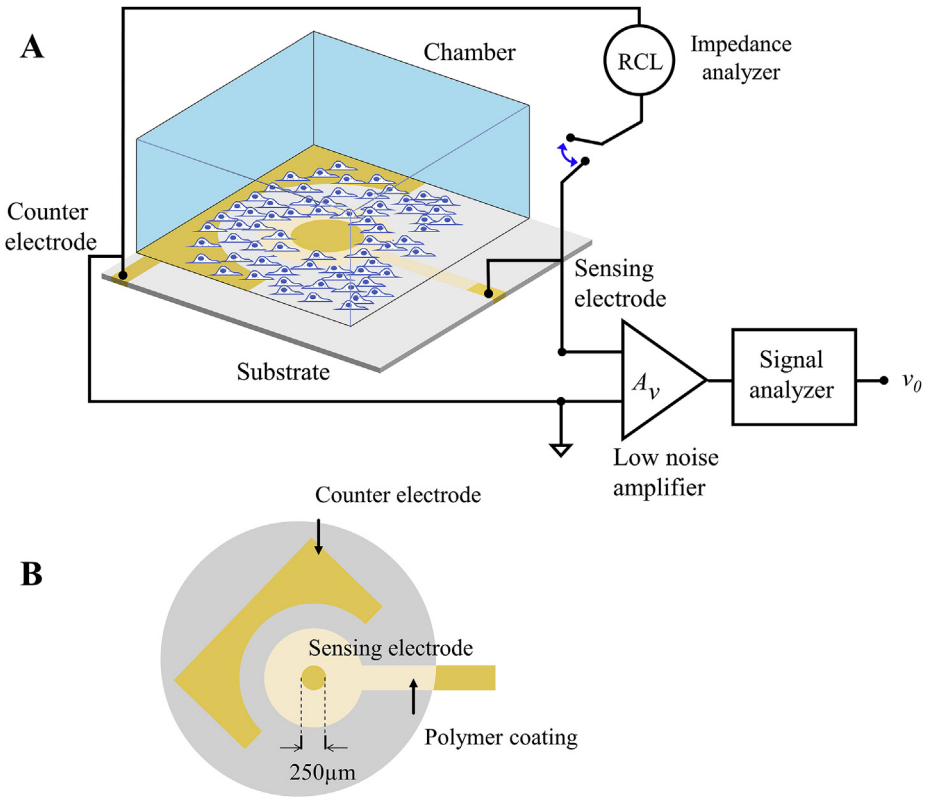

Fig. 1. Sensing device and the electrical measuring set-up. (A) A schematic diagram of the sensing electrode geometry and the electrical connections to the measuring instrumentation. (B) Detailed schematic diagram of the electrode geometry. The active electrode area of the sensing electrode is defined by an opening in a polymer over layer that insulates the rest of the deposited gold from the electrolyte solution. (For interpretation of the references to colour in this figure legend, the reader is referred to the Web version of this article.)

of signals, both spatially and temporally. Despite some molecular mechanistic insights, it remains unclear how the various, chemical, mechanical and, potentially, electrical signals from neighboring cells become integrated to allow coordinated multicellular movements. There is evidence that this coordination may involve multicellular Ca^{2+} waves transmitted from cell to cell (Giannone et al., 2002; Klepeis et al., 2001). Ion channels (migration-associated transportomes) are instrumental in cell migration (Schwab and Stock, 2014), playing multiple roles; i) they act as a sensor for extracellular guidance cues (Gurnett and Hedera, 2007), ii) they mediate the influx of Ca^{2+} that controls actin polymerization (Veksler and Gov, 2009), and iii) they induce cell shape changes and membrane depolarization (Schwab et al., 2012). The study of ion channels essentially relies on the use of patch clamp techniques (Chen et al., 2009). This technology requires precision micromanipulation and operators with large experience and skills. The integration of patch clamp methods with a migration experiment is also not trivial. In this context extracellular measurements of the ionic fluctuation during migration of cell populations are a simpler technique and may provide direct insight into the way the cells coordinate their collective movement.

Herein we present a cell-based biosensor that relies on extracellular electrophysiological cooperative cell activity. The method provides a set of relevant parameters about cell migration, namely speed and the kinetics of the establishment of cell-cell connections.

In order to validate the electrophysiological based method, we use a standard and well-accepted technique to measure cell migration. This method know as electrochemical cell impedance spectroscopy (ECIS) relies on the change of the electrode impedance with cell coverage (Giaever and Keese, 1991; Wegener et al., 2000). Cell migration experiments using the ECIS method were carried out in parallel with electrophysiological time traces. The spectral properties of the recorded signals, namely the frequency and the signal duration, were correlated with cell confluence estimated by the ECIS method. We used C6 glioma cells as a model system. The C6 system has similarities with primary brain tumors, gliomas, and the role of ion channels in the promotion of cell motility has been particularly well studied using patch clamp (Bowman and Lohr, 1996) and optical fluorescence methods (Pollak et al., 2017; Bose et al., 2015; Cuddapah et al., 2014; Mcferrin and Sontheimer, 2006; Pollak et al., 2017; Wang et al., 2015).

2. Material and methods

2.1. Cell lines and chemicals

Rat glioma C6 cells (American Type Culture Collection, USA) were cultured in F–12K nutrient medium supplemented with 15% fetal horse serum, 2.5% fetal bovine serum, and 1% penicillin and streptomycin. The cells were maintained under aseptic conditions at 37 °C in a CO_2 incubator (Thermo Scientific Midi 40) containing a 5% CO_2/air gas mixture that was automatically controlled. UV sterilization was accomplished using an Olympus TH4-200 and the exposure time was 5 minutes, to prevent damage to the vessel sealant.

The C6 glioma cells were harvested from the culture plates using a cell scraper and diluted in culture medium to yield a cell suspension (in F–12K nutrient mixture) containing from 50,000 up to 300,000 cells. The cell suspension was used to seed the device, which was maintained in an incubator for 24 hours until a confluent monolayer that covered the entire surface of the device, including the sensing electrode, was obtained. The cells were mechanically removed from the sensing electrode using a hand-held scraper. The detached cells were then washed using several changes of cell culture medium.

Digital images of the migrating cells were captured using an Olympus BX41 and a camera coupled to a computer.

C6 glioma cell number and viability was assessed using a Neubauer chamber and a trypan blue live/dead exclusion assay. The average viability of cultures remained at all points ~80% (± 12%). The cells were highly viable during the migration experiments.

2.2. Exposure to chemicals

A calcium-chelating agent, ethylene glycol-bis(β-aminoethyl ether)-N,N,N′,N′-tetraacetic acid (EGTA), was used to quelate extracellular Ca^{2+}, and the effects on cell signaling behavior were subsequently assessed. The culture medium bathing the C6 glioma cells was removed and replaced by a culture medium containing 10 mM EGTA. Cells were exposed to EGTA for 30 minutes, then the medium was removed, and the cells were washed twice with fresh culture medium.

2.3. Electrical measurements

The experimental electrical set-up was specifically designed for ultrasensitive detection and is schematically represented in Fig. 1(A). External interference was minimized through the use of a Faraday cage and low noise cables. Extracellular voltage measurements were carried out using a low-noise voltage amplifier (SR 560, Stanford Research) and a dynamic signal analyzer (35670A, Agilent). Small-signal impedance measurements were carried out using an RCL meter Fluke PM 6306.

Electrodes were purchased from Applied Biophysics (USA). The sensing device was comprised of a patterned gold electrode on a polycarbonate (PET) substrate. Each sensing device was in an individual chamber to permit multiple individual assays simultaneously. Each chamber has a substrate area of 0.8 cm^2, and a single centrally located circular 250 μm diameter electrode. A detailed schematic diagram of the electrode geometry is shown in Fig. 1(A). The region surrounding the sensing electrode represents an insulating polymer (photoresist) layer that partially coats the sensing electrode. The underlying gold layout connects the active electrode area to contact areas outside the measuring chamber. The device also has a large counter-electrode located at a distance of 2.5 mm from the sensing electrode. Both sensing and counter electrode were made of a thin gold film deposited on top of the PET substrate.

2.4. Statistics

Impedance and voltage signal measurements were repeated three times with an identical number of cells. Exposure of cells to the calcium-chelating agent (EGTA) was performed three times.

Statistical analysis of data was performed using a Student t-test in Matlab. The experimental data is reported as mean ± relative standard deviation (RSD).

3. Results

A schematic diagram of the electrode geometry and the electrical connections to the measuring instrumentation is depicted in Fig. 1 (A). The device utilized in the study was purchased from Applied Biophysics. The geometry of the patterned electrode system is schematically represented in Fig. 1 (B). An individual measuring chamber with a single centrally located circular 250 μm diameter electrode was used to detect the electrical activity as the C6 cells migrated from the surrounding area onto the central sensing electrode.

To study the migration of C6 glioma cells, typically a population of 3750/mm^2 cells was seeded onto the device. Lower cell densities of 625/mm^2 and 1250/mm^2 cells were also used in some experiments. An adherent and confluent monolayer was established and covered the entire device 24 hours after cell seeding. Cells adherent to the sensing electrode were mechanically removed, as described in the materials and methods section.

Fig. 2 (A) shows the migrating C6 cells coating the sensing electrode. The migration of C6 glioma cells onto the electrode was confirmed by optical microscopy and by the ECIS method. The ECIS method relies on the change of the cell/substrate interfacial resistance as the C6 glioma cells cover the electrode. Fig. 2 (B) shows the changes in the electrode/cell interface impedance with time as cells migrate

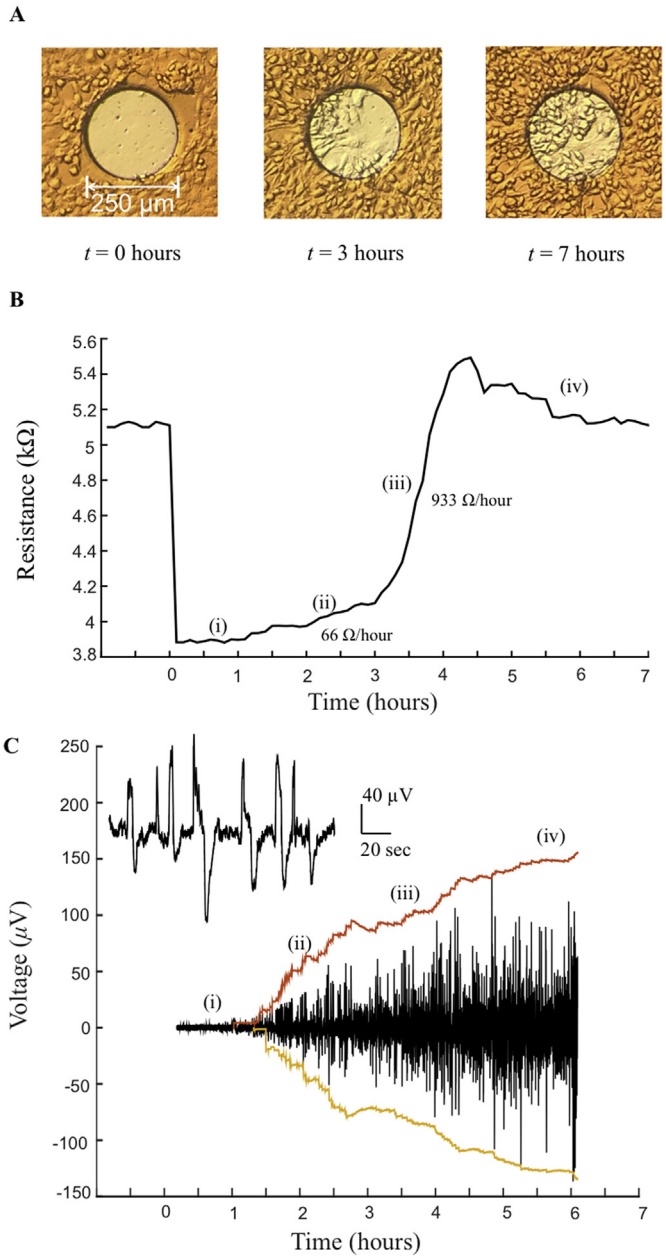

Fig. 2. Migration of C6 glioma cells monitored by microscopy, electrophysiological measurements and small signal impedance measurements. (A) A sequence of photographs showing the migration of the C6 glioma cells onto the central sensing electrode. (B) The time dependence of the electrical resistance measured at a frequency of 10 kHz (ECIS method). (C) The time dependence of the electrophysiological signals generated by the C6 glioma cells as they migrate onto and cover the sensing electrode surface. The inset in (C) gives a detailed view of the signals recorded 3 hours after the start of the experiment. The red line represents the cumulative sum of the signals over intervals of 5 minutes. (For interpretation of the references to colour in this figure legend, the reader is referred to the Web version of this article.)

onto the sensing electrode. The measurement of impedance started with a population of confluent cells on top of the sensing electrode. The high value of resistance at t < 0 s confirmed that the electrode was covered with cells. Cells were then mechanically detached from the electrode to leave the sensing electrode surface free of cells. Damaged and dead cells were removed by several washes with cell culture medium. Only healthy cells were left on the device. The mechanical induced wound often extended over an area larger than the sensing electrode area; therefore, the electrophysiological recording was only initiated when a

healthy cell population had reached the border of the sensing electrode.

The removal of cells from the sensing electrode meant that the insulating property of the living cells was lost and the impedance dropped. Thereafter, the increased resistance revealed the migration of cells onto the sensing electrode. The final values obtained for the resistance confirmed that full cell confluence was achieved. Since cells travel from all directions onto the circular electrode, it was assumed that, to reach full coverage, the cells had to travel a distance equal to the electrode radius (125 μm). Assuming a spatially uniform cell migration rate, the average cell migration speed was estimated to be 28 μm/h in agreement with values previously reported in the literature for C6 glioma cells (Joy et al., 2003).

Next, we show that if we measure the bioelectrical fluctuations, we also obtain information about the migration speed. The electrophysiological data is in close agreement with the values provided by the ECIS method. Moreover, because the bioelectrical activity is strongly related with the cell-cell connections, the bioelectrical fluctuations also reveal how the cell connectivity evolves during the migration of the cells.

Fig. 2 (C) shows a typical time trace of electrophysiological activity as the cells migrate onto the sensing electrode. The time trace is divided into several regions (i – iv). In the first region (i) the signal amplitude increases with time and this stage corresponds to the onset of cell migration onto the sensing electrode. Since the signals are biphasic, this gives rise to a time trace with a V-like shape. During this period of approximately 2.5 hours the signal amplitude increases with time. The V-shape then evolves to a region (ii) where the signal amplitude stabilizes and reaches a plateau. The onset of the plateau on the electrophysiological trace coincides with the onset of the plateau of the ECIS curve shown in Fig. 2 (B). This confirms that the saturation on the amplitude of the electrophysiological signals occurs when cell confluence is reached. Both the cell-substrate impedance (ECIS method) and the bio-signal amplitude reached a saturation plateau in the same time span.

For periods longer than 6 hours the electrophysiological activity is characterized by bursts intercalated with short periods of weak activity as illustrated in region (iv) in Fig. 2 (C).

To clearly demonstrate the temporal evolution of the signals, the total migration time was divided into smaller time intervals of 5 minutes and then the cumulative sum of the signals over this period was established. This cumulative sum produced an average time evolution of the signal amplitude, reflecting its increase. The continuous red line in Fig. 2 (C) shows the cumulative sum of the signal amplitude as a function of time. Initially, as shown in region (i) of Fig. 2 (C), the electrical noise of the empty electrode was approximately 4 μV peak-to-peak. Discrete signals began to be detected approximately 80 minutes after cell removal (Fig. 2 (C), region (ii)), with the amplitude of the signals rising linearly from 5 to 8 μV up to 20 μV. For times between 3 and 3.5 hours the signal amplitude remained approximately stable, around an average value of 20 μV and corresponded to a plateau (iii). The first plateau at 3–3.5 hours was followed by an increase in signal amplitude, reaching a second plateau of higher amplitude, 4.5 hours after the start of the experiment (region (iv)).

The inset in Fig. 2 (C) is a representative example of a short time trace recorded during the migration of the C6 glioma cells. Signal shapes were often biphasic, although monophasic signals with either upward or downward voltage fluctuations were also observed. Across time the signals associated with C6 migration had an overall symmetrical shape, centered on a positive offset potential and oscillating with time. To facilitate visualization of the data, we arbitrarily considered the offset potential to be zero volts, as shown in Fig. 2 (C).

Five migration experiments were carried out for different cell densities. Fig. 3 illustrates how C6 glioma cell density affects the shape of the electrophysiological time trace. The first two electrophysiological traces (#1 and #2) correspond to a non-confluent cell population. The inset photographs in Fig. 3 (C) illustrates the cell density used in experiment #2 and #4. As the C6 glioma cells migrated onto the sensing electrode, the V-shaped signal was low intensity across time. For the experiments #3 to #5 the cells at the border of the sensing electrode were closely packed. Highly confluent cell populations produced an electrophysiological time trace with well-defined V-shaped signals; how this is related to the increasing number of cells connected by tight junctions is subsequently discussed.

In the following section it is demonstrated how the bioelectrical signal properties namely the frequency (f), duration (T_s) and amplitude (A_S) provide quantitative information about migration speed and cell-cell connectivity. As more cells migrated onto the sensing electrode, the frequency, amplitude and the signal duration increased. The histogram in Fig. 4 (A) presents the change in signal frequency with time. The frequency increased from 30 signals per hour ($f = 8.3$ mHz) to approximately 100 signals per hour ($f = 28$ mHz) when cell confluence was reached. The histogram in Fig. 4 (B) shows the evolution of the signal duration as the cells migrate onto the sensing electrode. Initially, the signals had an average duration of 9 seconds. After 5.5 hours the signal duration rose rapidly and abruptly to an average of 18 seconds and then remained approximately constant for the rest of the time.

Assuming that the saturation of the signal duration at 18 seconds corresponds to full electrode coverage by the cells, then there is a delay of 1.5 hours in respect to the time required to reach the plateau in resistance of the ECIS method (see Fig. 2 C). This delay between the plateau in electrophysiological and ECIS recordings may be explained by the fact that the ECIS method is only sensitive to cell coverage while electrophysiological signals require the establishment of cell-cell connections.

Fig. 5 shows the linear relationship between signal duration and amplitude. The straight-line is a polynomial fit to the data and has a slope of 3.043 ± 0.70 μV/s. This relationship is a strong indication that discrete signals are a result of cell-synchronized behavior.

Having demonstrated that electrophysiological signals can be used as a quantitative and reliable method to gain insight into the way cells establish connections with neighbor cells, we then explored how the C6 glioma cell electrophysiological activity is turned-off if the cell connectivity is disrupted by exposure to chemicals. A calcium-chelating agent, ethylene glycol-bis(β-aminoethyl ether)-N,N,N′,N′-tetraacetic acid (EGTA), was added to the C6 glioma cell culture to disturb cellular Ca^{2+} concentrations and break the cell-cell connections. The effect of replacing the cell culture medium with a culture medium containing EGTA (10 mM) is presented in Fig. 6 (A). Before the exposure of C6 glioma cells to the medium containing EGTA, the cells exhibited a strong electrophysiological activity. However, upon EGTA exposure the C6 glioma cell activity was immediately silenced and remained so for the full period of exposure to EGTA (30 minutes). When the EGTA-containing medium was removed and replaced by normal culture medium the C6 glioma cells became electrically active thirty minutes after the EGTA removal. The recovery of electrophysiological activity followed a pattern in which the signal amplitude increased with time. The exposure of C6 glioma cells to EGTA was replicated in three different experiments and the outcome was consistent. Fig. 6 (B) shows the signal data in the frequency domain and reveals how much of the signal lies within a given frequency band. The recorded signals of the EGTA recovering C6 glioma cells were not periodic, and so no discrete spectral lines were present in the frequency representation. The PSD in Fig. 6 (B) also shows that the region below 1 Hz did not recover totally. Furthermore, the histogram in Fig. 6 (C) shows that after 1.5 hours the frequency of the signals was still lower than before the EGTA exposure. It is noteworthy that the few signals recorded under EGTA exposure were weak and had amplitude only slightly above the thermal noise.

It has been reported that calcium is involved in the establishment of gap junctions (Fujii et al., 2017; Mettang et al., 2018; Peracchia, 1978; Szabó et al., 2017), although the processes that cause the inhibition of the signaling mechanisms seen in the present study are elusive. EGTA chelates all the calcium in the cell culture medium, depriving cells of

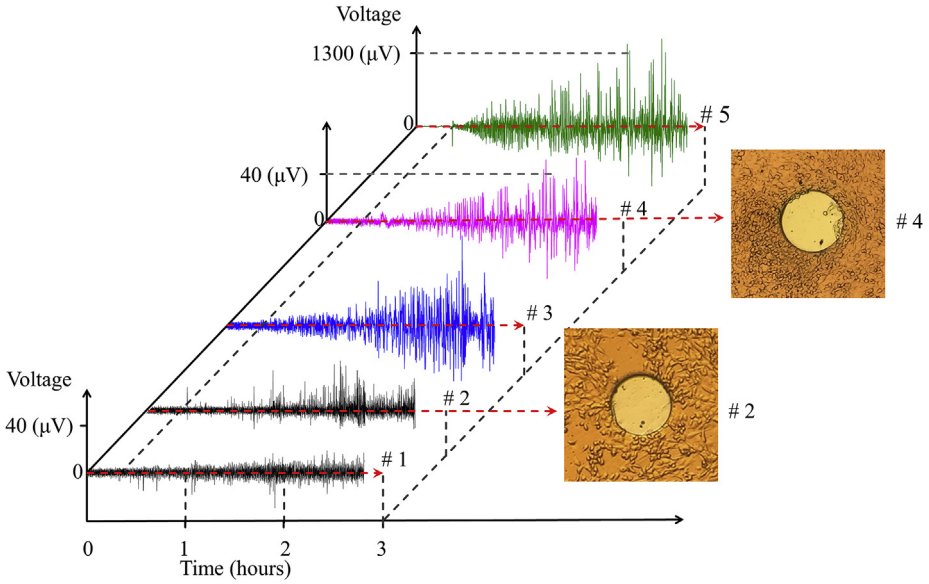

Fig. 3. Individual electrophysiological time traces recorded with varying cell confluence. The cell seeding density was varied from 625 cells/mm^2 (experiment #1) to more than 3750 cells/mm^2 (experiment #5). The photographs show the level of cell confluence around the recording electrode for experiments #2 and #4.

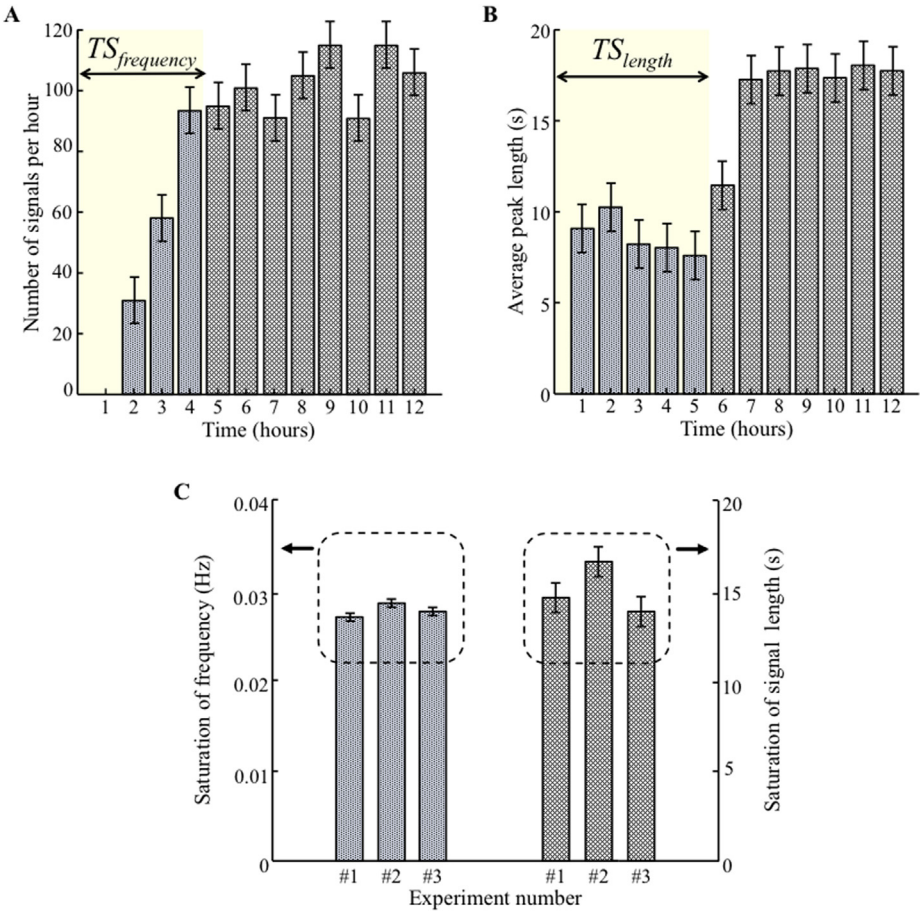

Fig. 4. Evolution of the bioelectrical signal properties with migration time. (A) Evolution of signal frequency with time (based on n = 3 independent experiments with replicate samples). (B) Changes in the average signal length with migration time. (C) Statistical variations in the time to reach saturation of signal frequency ($TS_{frequency}$) and signal length (TS_{length}). Note that both $TS_{frequency}$ and TS_{length} are good indicators of cell migration time. The error bars are the relative standard deviation.

free Ca^{2+} and may therefore inhibit or even disrupt calcium signaling. To assess if cell morphology or gap junctions were disrupted, the impedance was also measured upon EGTA exposure. Fig. 6 (D) shows the frequency dependence of the impedance of a confluent cell population, before and after EGTA exposure. Under EGTA exposure, a small decrease in the impedance was observed. The inset in Fig. 6 (D) shows the time dependence of the resistance change, measured at 10 kHz. Immediately after EGTA exposure the resistance dropped abruptly and remained low. Upon washout of EGTA the electrical resistance began to recover with time, attaining a plateau of 16 kΩ after 1.5 hours. This capacitance plateau was equivalent to a 90% recovery of the original resistance value.

A control experiment, in which EGTA was added to the cell culture medium in the absence of cells, was also carried out. Fig. 6 (E) shows

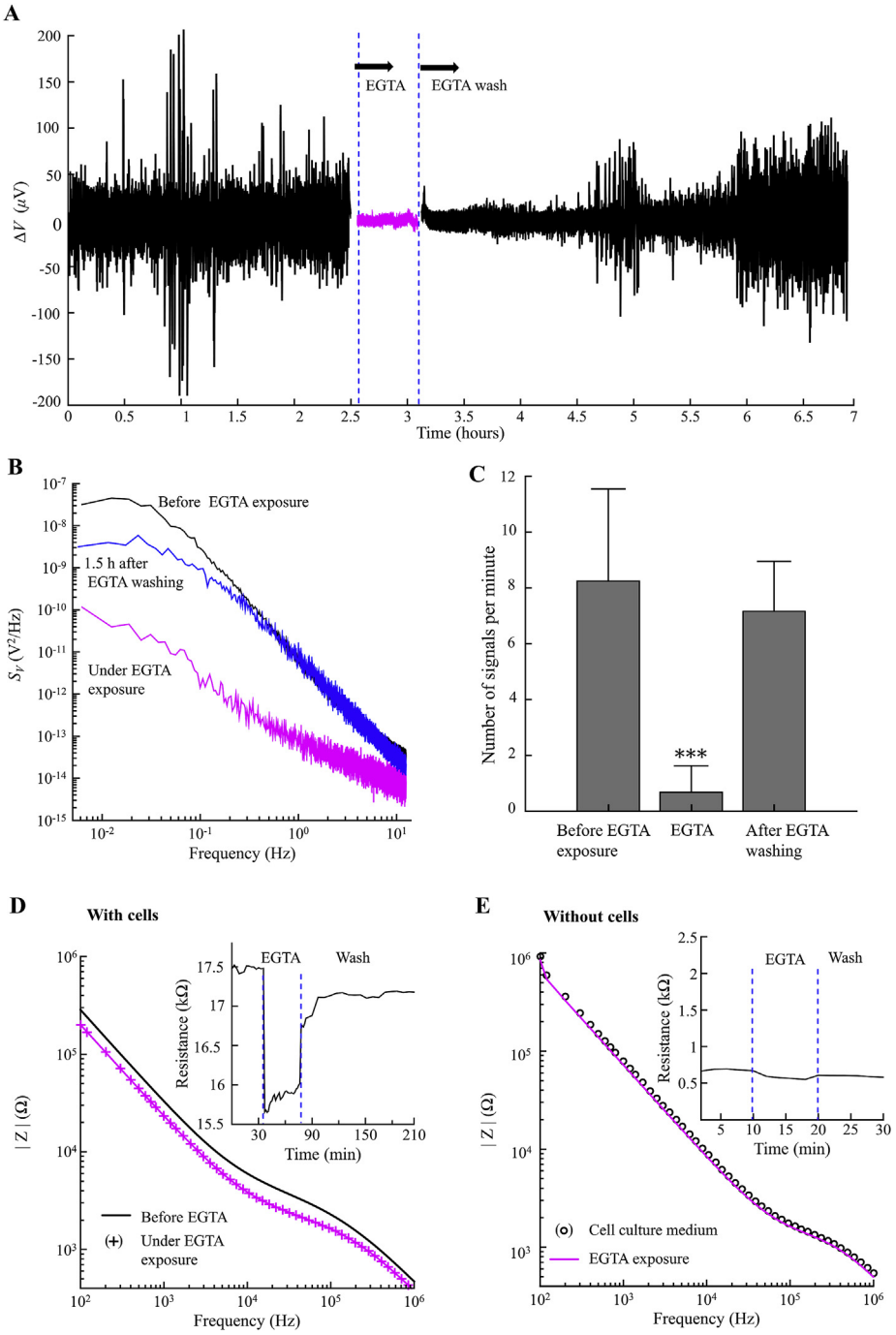

Fig. 5. Electrical signals of a C6 glioma cell population in the presence of EGTA. (A) Long-term recording of C6 glioma cell activity before, during and after EGTA exposure. (B) Frequency dependence of the noise power density in voltage. The black line represents the values before EGTA exposure; the pink line represents the recording under EGTA exposure and the blue line represents 1.5 h after washing out the EGTA. (C) A histogram showing the number of signals per minute before, during and after washout of EGTA. The graphs in (D) and (E) represent the changes in impedance when EGTA was added. (D) shows how the impedance of the electrode coated with C6 glioma cells responds to EGTA addition and (E) represents the impedance variation caused by addition of EGTA in the absence of cells. The inset in (D) and (E) represents the transient response of the electrode resistance at a fixed frequency of 10 kHz when EGTA is added. (For interpretation of the references to colour in this figure legend, the reader is referred to the Web version of this article.)

that there were no significant changes in the impedance of the electrode/cell interface. The inset shows the temporal evolution of the resistance measured at a frequency of 10 kHz. This confirmed that the change in impedance upon EGTA exposure was related to the presence of cells and not to a change in the electrolyte composition.

To visualize the effects of the calcium deprivation on the cell morphology, photographs were taken as a function of time under EGTA exposure. Fig. S1 (A) in the supplementary information illustrates the change in cell morphology upon EGTA exposure. Before exposure to EGTA the cells were adherent and exhibited a flattened shape with their membranes contiguous with neighboring cells. EGTA exposure caused an immediate change to a spherical cell shape and after 10 minutes cells no longer contacted with each other. Immunofluorescence assays were carried out to examine the integrity of tight junctions. The monoclonal antibody ZO-1 (zonula occludens-1 protein), a TJ-associated protein, was used to assess the stability of tight junctions. The tight junctions were evident as a green rim-like pattern around the individual control C6 glioma cells (Fig. S1 (B)) and narrow and well-defined junctional areas contiguous between neighboring cells were identified. Upon calcium chelation with EGTA the green fluorescence was lost from the contact point between adjacent cells and was instead in the cell cytoplasm indicating that the tight junctions were disrupted. One hour after restoration of normal Ca^{2+} concentrations cell-to-cell contacts were restored and positive anti-ZO-1 fluorescence was detected in contiguous regions between the C6 glioma cells (see Fig. S1 (B)). In summary, short-term treatment of confluent C6 glioma cells with EGTA induced the loss of TJs and was associated with a significant reduction in electrophysiological activity.

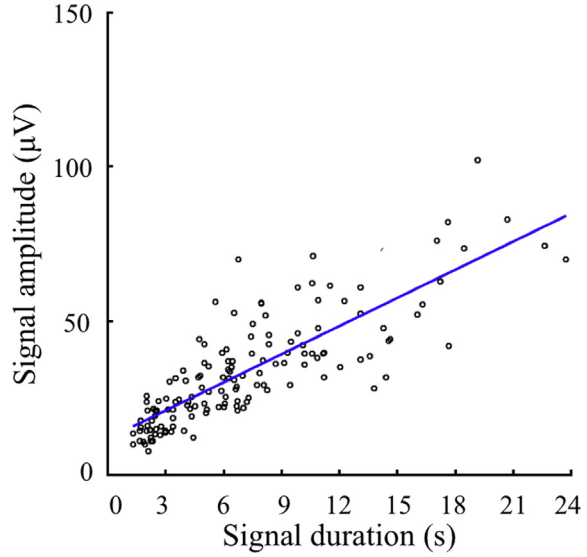

Fig. 6. The relationship between signal duration and the signal amplitude. Long lasting signals were higher in amplitude. The straight-line fitted to the data had a slope of 3.03 ± 0.70 μV/s.

5. Discussion

The new methodology presented in this article has a number decisive advantages compared with other well-established approaches to study cell migration. Cell migration speed can easily be determined by simpler and less expensive techniques such as scratch assays or wound healing assays. The measurement of ultra-weak extracellular signals with low noise and high gain voltage amplifiers is far more complex than the simple video camera or even impedance meters used in the ECIS method. If the goal is to obtain only the cell migration speed, then bioelectrical signal measurements are a cumbersome and expensive approach. However, if the aim is to characterize the underlying mechanisms of cell migration and for instance, gain insight into how the cells connect to each other during migration and about the signals they share to coordinate their movements, then bioelectrical measurements are an ideal tool. Knowing that electrophysiological measurements basically measure the activity of ion-channels, it could be argued that immunofluorescence assays are the gold standard to probe ion-channel activity. However, the incubation with fluorophores and light exposure may disturb cell activity. Furthermore, the relatively short lifetime of the fluorophores impedes the recording of ion channel activity for the extensive periods of time (> 2 hours) that often are required to reach cell confluence on the sensing electrode. Therefore, the primary advantage of the novel methodology presented to study cell migration is that bioelectrical extracellular measurements provide real time and non-invasive information about the cell-cell connectivity and about the synchronization of cells during the migration. These features permit collective and organized migration to be distinguished from solitary cell migration. As such the technique significantly advances the state-of-the-art in cell migration experiments.

A large number of migration processes are a collective phenomenon that requires communication and coordination among groups of cells. For example, in a study by Khain E et al. (2009) about clustering dynamics of glioma cells on a surface, it was reported that some cell lines formed clusters in regions of low cell density and that this increased their proliferation rate. Based on the findings reported here, electrophysiological recordings could provide important insights into clustering dynamics of cancer cells and the formation and propagation of cancer metastasis.

Although we used C6 glioma cells as a prototype system, it should be possible to extend our studies to other cell types. Finally, the possibility of measuring tumor cell migration using electrophysiological recordings could be exploited to identify antimigratory strategies not disclosed by other *in vitro* methods. The ion channels must be directly involved in the generation of the recorded extracellular signals. Considering the vast array of therapeutic drugs that target ion channels (Lipscombe and Wyllie, 2018), and modulate the membrane potential of malign tissues our approach may provide a new, cheap and quick active compound screening approach. It is clear that ion channels are a worthy target of future research, with a potential impact in pharmaceutical screening and also as a model system for understanding the general behavior of cells.

The collective migration of the C6 cells detected in the present study must be favored by forces exerted by the confluent cells that push the cells located at the border into the cell-free region. This type of directed cell migration is known as durataxis (DuChez et al., 2019). Chemotaxis and haptotaxis are other effects that can polarize or force cells to move persistently in a specified direction. The consequence of this directional migration on the bioelectrical activity should be considered in future experiments.

It has been reported that cancer cells also exhibit temperature fluctuations reaching 285 mK in amplitude (Yang et al., 2017). Although, these oscillations are of very low frequency, they occur in a timescale that is three orders of magnitude slower than the voltage fluctuations reported here. The discrepancy in the timescale of the phenomenon means a link between the two types of oscillations could not be established.

6. Conclusions

This article demonstrates that electrophysiological recordings in populations of C6 glioma cells are directly correlated with the migration of the cells. As C6 cells migrate onto a sensing area free of cells, they establish cell-cell connections forming synchronized cell clusters that generate discrete bioelectrical signals. The frequency, amplitude and duration of the signals increase with the number of cells connected to each other. When cell confluence is reached there is a maximum number of cells synchronized, therefore, the signal amplitude and frequency saturate at well-defined value. The time at which the signal parameters are saturated is a good indicator of the total migration time. This migration was confirmed by independent ECIS measurements. The relationship between confluence and the synchronized cellular bioelectrical activity means that measurements of cell signals can distinguish collective and organized migration over solitary cell migration. Future advances using this electrophysiological approach combined with other methods will hopefully lead to the development of a new generation of anticancer drugs that target cell motility.

CRediT authorship contribution statement

Sanaz Asgarifar: Investigation, Formal analysis, Writing - original draft. **Ana L.G. Mestre:** Investigation, Writing - original draft. **Rute C. Félix:** Investigation, Formal analysis, Writing - review & editing. **Pedro M.C. Inácio:** Software. **Maria L.S. Cristiano:** Methodology, Writing - review & editing. **Maria C.R. Medeiros:** Conceptualization, Writing - review & editing. **Inês M. Araújo:** Writing - review & editing. **Deborah M. Power:** Methodology, Formal analysis, Writing - review & editing. **Henrique L. Gomes:** Conceptualization, Supervision, Formal analysis, Writing - review & editing.

Declaration of competing interest

The authors declare that they have no known competing financial interests or personal relationships that could have appeared to influence the work reported in this paper.

Acknowledgments

We thank Prof. Michele Zoli from the University of Modena and Reggio Emilia in Italy and to Prof. David Martin Taylor from the University of Bangor, North Wales, in UK for fruitful discussions.

We gratefully acknowledge support from the Portuguese Foundation for Science and Technology (FCT), through the projects PTDC/EEI-AUT/5442/2014 ("Implantable organic devices for advanced therapies" (INNOVATE)), UID/EEA/50008/2019 (Instituto de Telecomunicações, IT, UID/BIM/04773/2019 (Centro de Investigação em Biomedicina)) and UID/Multi/04326/2019 (Centro de Ciências do Mar, CCMar) RCF acknowledges the auxiliary research contract with the Universidade do Algarve.

Appendix A. Supplementary data

Supplementary data to this article can be found online at https://doi.org/10.1016/j.bios.2019.111708.

References

Banerjee, P., Bhunia, A.K., 2010. Biosens. Bioelectron. 26, 99–106.
Bose, T., Cieślar-Pobuda, A., Wiechec, E., 2015. Cell Death Dis. 6, e1648.
Bowman, C.L., Lohr, J.W., 1996. Glia 18, 161–176.
Cabello, M., Ge, H., Aracil, C., Moschou, D., Estrela, P., Quero, J.M., Pascu, S.I., Rocha, P.R.F., 2019. Sensors 19, 1–11.
Chen, P., Zhang, W., Zhou, J., Wang, P., Xiao, L., Yang, M., 2009. Prog. Nat. Sci. 19, 153–160.
Cuddapah, V.A., Robel, S., Watkins, S., Sontheimer, H., 2014. Nat. Rev. Neurosci. 15, 455–465 5.
DeBusschere, B.D., Kovacs, G.T.A., 2001. Biosens. Bioelectron. 16, 543–556.
DuChez, B.J., Doyle, A.D., Dimitriadis, E.K., Yamada, K.M., 2019. Biophys. J. 116, 670–683.
Fujii, Y., Maekawa, S., Morita, M., 2017. Sci. Rep. 7, 13115.
Giaever, I., Keese, C.R., 1991. Proc. Natl. Acad. Sci. U.S.A. 88, 7896–7900.
Giannone, G., Rondé, P., Gaire, M., Haiech, J., Takeda, K., 2002. J. Biol. Chem. 277, 26364–26371.
Gov, N.S., 2014. Cell Matrix Mech. 219–238.
Gross, G.W., Rhoades, B.K., Azzazy, H.M.E., Wu, M., 1995. Biosens. Bioelectron. 10, 553–567.
Gurnett, C.A., Hedera, P., 2007. Arch. Neurol. 64 (3), 324–328.
Hierlemann, A., Frey, U., Hafizovic, S., Heer, F., 2011. Proc. IEEE 99, 252–284.
Jiang, J., Li, L., He, Y., Zhao, M., 2015. Burn. Trauma 1, 21–26.
Johnstone, A.F.M., Gross, G.W., Weiss, D.G., Schroeder, O.H.U., Gramowski, A., Shafer, T.J., 2010. Neurotoxicology (Little Rock) 31, 331–350.
Joy, A.M., Beaudry, C.E., Tran, N.L., Ponce, F.A., Holz, D.R., Demuth, T., Berens, M.E., 2003. J. Cell Sci. 116 (21), 4409–4417.
Klepeis, V.E., Cornell-Bell, A., Trinkaus-Randall, V., 2001. J. Cell Sci. 114, 4185–4195.
Lipscombe, D., Wyllie, D.J.A., 2018. Curr. Opin. Physiol. 2, iv–vii.
Mcferrin, M.B., Sontheimer, H., 2006. Neuron Glia Biol. 39–49.
Medeiros, M.C.R., Mestre, A., Inácio, P., Asgarif, S., Araújo, I.M., Hubbard, P.C., Velez, Z., Cancela, M.L., Rocha, P.R.F., de Leeuw, D.M., Biscarini, F., Gomes, H.L., 2016. Sens. Biosens. Res. 10, 1–8.
Mestre, A.L.G., Cerquido, M., Inácio, P.M.C., Asgarifar, S., Lourenço, A.S., Cristiano, M.L.S., Aguiar, P., Medeiros, M.C.R., Araújo, I.M., Ventura, J., Gomes, H.L., 2017a. Sci. Rep. 7, 14284.
Mestre, A.L.G., Inácio, P.M.C., Elamine, Y., Asgarifar, S., Lourenço, A.S., Cristiano, M.L.S., Aguiar, P., Medeiros, M.C.R., Araújo, I.M., Ventura, J., Gomes, H.L., 2017b. Front. Neural Circuits 11.
Mettang, M., Meyer-Pannwitt, V., Karpel-Massler, G., Zhou, S., Carragher, N.O., Föhr, K.J., Baumann, B., Nonnenmacher, L., Enzenmüller, S., Dahlhaus, M., Siegelin, M.D., Stroh, S., Mertens, D., Fischer-Posovszky, P., Schneider, E.M., Halatsch, M.E., Debatin, K.M., Westhoff, M.A., 2018. Sci. Rep. 8, 5527.
Pan, Y., Hu, N., Wei, X., Gong, L., Zhang, B., Wan, H., Wang, P., 2019. Biosens. Bioelectron. 130, 344–351.
Pancrazio, J.J., Borkholder, D.A., 1999. Ann. Biomed. Eng. 27 (6), 697–711.
Peracchia, C., 1978. Nature 271, 669–671.
Pollak, J., Rai, K.G., Funk, C.C., Arora, S., Lee, E., Zhu, J., Price, N.D., Paddison, P.J., Ramirez, J.M., Rostomily, R.C., 2017. PLoS One 12 (3), e0172884.
Rocha, P.R.F., Medeiros, M.C.R., Kintzel, U., Vogt, J., Araújo, I.M., Mestre, A.L.G., Mailänder, V., Schlett, P., Dröge, M., Schneider, L., Biscarini, F., de Leeuw, D.M., Gomes, H.L., 2016. Sci. Adv. 2, e1600516.
Schwab, A., Fabian, A., Hanley, P.J., Stock, C., 2012. Physiol. Rev. 92, 1865–1913.
Schwab, A., Stock, C., 2014. Philos. Trans. R. Soc. Lond. B Biol. Sci. 369, 20130102.
Spira, M.E., Hai, A., 2013. Nat. Nanotechnol. 8, 83–94.
Szabó, Z., Héja, L., Szalay, G., Kékesi, O., Füredi, A., Szebényi, K., Dobolyi, Á., Orbán, T.I., Kolacsek, O., Tompa, T., Miskolczy, Z., Biczók, L., Rózsa, B., Sarkadi, B., Kardos, J., 2017. Sci. Rep. 7, 6018.
Theveneau, E., Mayor, R., 2012. Curr. Opin. Cell Biol. 24, 677–684.
Veksler, A., Gov, N.S., 2009. Biophys. J. 97, 1558–1568.
Wang, R., Gurguis, C.I., Gu, W., Ko, E.A., Lim, I., Bang, H., Zhou, T., Ko, J.H., 2015. Sci. Rep. 5, 11593.
Wegener, J., Keese, C.R., Giaever, I., 2000. Exp. Cell Res. 259, 158–166.
Yang, F., Li, G., Yang, J., Wang, Z., Han, D., Zheng, F., Xu, S., 2017. Sci. Rep. 7, 1–12.
Ye, Y., Guo, H., Sun, X., 2019. Biosens. Bioelectron. 126, 389–404.